Available online at www.sciencedirect.com

ScienceDirect

Ceramics International 40 (2014) 3117–3122

CERAMICS INTERNATIONAL

www.elsevier.com/locate/ceramint

Synthesis and luminescence of Y_2O_3:Eu^{3+} inorganic–organic hybrid nanostructures with thenoyltrifluoroacetone

Lu Ji[a], Nan Chen[a], Guoping Du[a,*], Mingming Yan[a], Wangzhou Shi[b,**]

[a]School of Materials Science and Engineering, Nanchang University, Nanchang, Jiangxi 330031, China
[b]Department of Physics, Shanghai Normal University, Shanghai 200234, China

Received 21 September 2013; received in revised form 28 September 2013; accepted 30 September 2013
Available online 8 October 2013

Abstract

Cubic Y_2O_3:Eu^{3+} nanoparticles with a size about 32 nm were synthesized using a facile hydrothermal method followed by an annealing process. As expected, the Y_2O_3:Eu^{3+} nanoparticles had a broad Eu–O excitation band ranging from 200 nm to 285 nm peaking at about 260 nm. The Y_2O_3:Eu^{3+} nanoparticles were then used to fabricate the inorganic–organic hybrid nanostructures with thenoyltrifluoroacetone (TTA). The Y_2O_3:Eu^{3+}–TTA hybrid nanostructures exhibited a new strong excitation band ranging from 280 nm to 390 nm peaking at about 368 nm. This new excitation band was attributed to the energy transfer mechanism of the Y_2O_3:Eu^{3+}–TTA hybrid system. It is interesting to note that this energy transfer mechanism had a close interaction with the Eu–O excitation of Y_2O_3:Eu^{3+} nanoparticles. The phase structures, chemical bonding information, microstructural characteristics and luminescence properties were investigated.

Keywords: Y_2O_3:Eu^{3+}; Nanoparticle; Luminescence; Inorganic–organic hybrid system; Energy transfer

1. Introduction

Rare earth (RE) doped oxide nanoparticles have attracted intensive interest due to their unique luminescent properties, and have important applications in the areas of light-emitting device [1], laser [2], biological label [3] and many others. In particular, Eu^{3+}-doped Y_2O_3 phosphor has been paid much attention because of its high refractory property and chemical stability [4]. The Eu^{3+}-doped Y_2O_3 phosphor has been widely used in fluorescent lamps. Until now, much research work has been conducted to synthesize Eu^{3+}-doped Y_2O_3 (Y_2O_3:Eu^{3+}) nanoparticles [5–7] and especially to improve their luminescence properties [8,9]. It has been shown that nanocrystalline Y_2O_3:Eu^{3+} exhibit stronger luminescence than its bulk counterpart [10].

One of the most effective methods for improving the luminescence intensity of RE doped nanocrystalline phosphors is to decorate their surfaces with organic ligands. It has been shown that organic ligands can sensitize RE ions, especially the Eu^{3+} ions, via the "antenna effect". In this process, the organic ligand with a strong optical absorption ability is first excited by the excitation wavelength, and then the absorbed energy is transferred to the associated RE ions and results in efficient emission via the RE ions [11,12]. Organic ligands, such as benzoic acid [13], 1,2,4,5-benzenetetracarboxylic acid [14], and β–diketonates [15,16] have been reported to be able to effectively sensitize RE ions in flourides can greatly enhance their luminescence properties. Up to now, however, little research has been done on the effect of organic ligand sensitization on the luminescence of the Y_2O_3:Eu^{3+} nanoparticles.

In this paper, Y_2O_3:Eu^{3+} nanoparticles were synthesized using a hydrothermal method followed by an annealing process. These Y_2O_3:Eu^{3+} nanoparticles were decorated with thenoyltrifluoroacetone (TTA) to form a kind of inorganic–organic hybrid nanostructures. A broad excitation band ranging from 280 nm to 390 nm was observed due to the sensitization mechanism via TTA. The effects of TTA content and synthesis conditions on the luminescent properties of the

*Corresponding author. Tel.: +86 791 3969553.
**Corresponding author.
E-mail addresses: guopingdu@ncu.edu.cn (G. Du), wzshi@shnu.edu.cn (W. Shi).

0272-8842/$ - see front matter © 2013 Elsevier Ltd and Techna Group S.r.l. All rights reserved.
http://dx.doi.org/10.1016/j.ceramint.2013.09.135

Y_2O_3:Eu^{3+}–TTA hybrid nanostructures were investigated in detail.

2. Experimental

2.1. Materials

Yttrium nitrate ($Y(NO_3)_3 \cdot 6H_2O$) and europium nitrate ($Eu(NO_3)_3 \cdot 6H_2O$) with a purity of 99.99% were used for the synthesis of Y_2O_3:Eu^{3+} nanoparticles. Urea, TTA and ethanol were of analytical grade and used without further purification.

2.2. Synthesis of Y_2O_3:Eu^{3+} nanoparticles

Y_2O_3:Eu^{3+} nanoparticles were synthesized using a hydrothermal and annealing method. In a typical procedure, 1.8 mmol $Y(NO_3)_3 \cdot 6H_2O$, 0.2 mmol $Eu(NO_3)_3 \cdot 6H_2O$ and 0.1802 g urea were dissolved in 2 ml deionized water with vigorous stirring. After stirring for 30 min, the mixture was heated in a water bath at 80 °C for 3 h to achieve a colloidal solution. The resulting solution was poured into a 50 ml Teflon-lined autoclave with a stainless-steel vessel, sealed, and heated at 120 °C for 16 h to obtain Y_2O_3:Eu^{3+} precursors. The precursors were then washed with ethanol and dried in an oven with an air atmosphere. The resulting powders were annealed at 850 °C in air for 2 h, 3 h, 4 h, and 5 h. After annealing, the powders were grinded with ethanol for 30 min to obtain the well-dispersed Y_2O_3:Eu^{3+} nanoparticles.

2.3. Synthesis of Y_2O_3:Eu^{3+}–TTA hybrid nanostructures

Appropriate amounts of Y_2O_3:Eu^{3+} nanoparticles and TTA were dissolved in 10 ml deionized water and 10 ml ethanol, respectively, followed by ultrasonic processing for 45 min. Mix the above two solutions together and stir for 2 h. The final mixture was kept at rest for 12 h. The precipitated powders were then washed with ethanol for three times to remove any residual TTA and dried in an oven with an air atmosphere. The chemical reaction between Y_2O_3:Eu^{3+} and TTA is illustrated in Fig. 1.

2.4. Characterization techniques

The crystal structure of the samples was investigated using the X-ray diffraction (XRD, Bruker D8 Focus) technique in the scanning range from 10° to 70° using Cu Kα radiation ($\lambda = 0.15406$ nm). Fourier transform infrared (FTIR) spectra were recorded on a FTIR spectrometer (Nicolet 380). The microstructures of the samples were studied using a field emission scanning electron microscope (FESEM, Hitachi S4800). The photoluminescence excitation and emission spectra were measured with a Hitachi F-4600 fluorescence spectrophotometer with a xenon lamp as the light source. All measurements were taken at room temperatures.

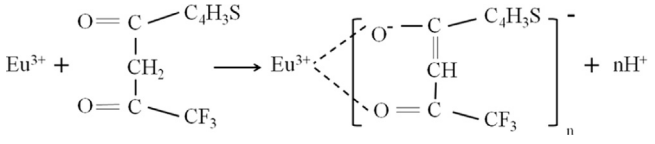

Fig. 1. The chemical reaction between Eu^{3+} ions on Y_2O_3:Eu^{3+} and TTA.

3. Results and discussion

3.1. Phase structure analysis

Fig. 2 shows the XRD pattern of the Y_2O_3:Eu^{3+} precursors annealed in air at 850 °C for 2 h, 3 h, 4 h, and 5 h. All of the XRD diffraction peaks in Fig. 1 can be readily indexed according to the cubic Y_2O_3 crystal structure (JCPDS: 41-1105), and no secondary phase was observed. This suggests that cubic Y_2O_3:Eu^{3+} particles were successful synthesized by the hydrothermal method followed by an annealing process.

The average crystallite size can be calculated by the Scherrer equation [17],

$$d = 0.89\lambda/\beta \cos\theta \quad (1)$$

where d is the crystallite size, 0.89 is the Scherrer constant, λ is the X-ray wavelength, β is the full width at half maximum of a diffraction peak, and θ is the diffraction angle. Table 1 shows the calculated average crystallite size of the Y_2O_3:Eu^{3+} particles after annealing at 850 °C for 2 h, 3 h, 4 h, and 5 h. All Y_2O_3:Eu^{3+} particles were found to nanocrystalline. As expected, longer annealing time resulted in relatively larger crystallite size of Y_2O_3:Eu^{3+}.

Fig. 3a shows the FESEM image of the Y_2O_3:Eu^{3+} nanoparticles which were obtained after annealing for 2 h. The TEM image of the Y_2O_3:Eu^{3+} nanoparticles were shown in Fig. 3b. It can be clearly seen that these Y_2O_3:Eu^{3+} nanoparticles had a near-spheroidal morphology. The HRTEM image (Fig. 3c) shows that the Y_2O_3:Eu^{3+} nanoparticles were monocrystals with an average particle size of about 32 nm, which is comparable to the average crystallite size calculated from the Scherrer equation (Table 1).

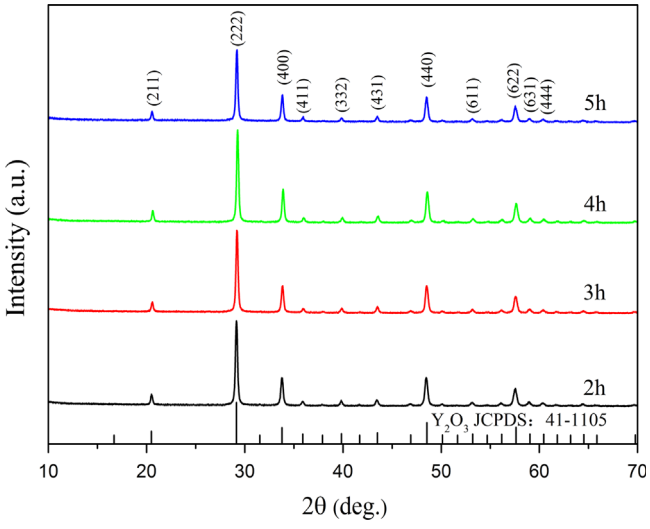

Fig. 2. XRD patterns for the samples annealed for 2 h, 3 h, 4 h and 5 h.

3.2. FTIR analysis of Y_2O_3:Eu^{3+}–TTA hybrid nanostructures

Fig. 4 shows the FTIR spectra of the Y_2O_3:Eu^{3+} nanoparticles, TTA, and Y_2O_3:Eu^{3+}–TTA hybrid nanostructures processed with different contents of TTA. The peaks at 559 cm^{-1} are assigned to the characteristic absorption peaks of Y_2O_3 [18]. This further confirms that the Y_2O_3 nanocrystals were synthesized. The new band at 1541 cm^{-1} for the Y_2O_3:Eu^{3+}–TTA samples is associated with the carbon–carbon double bond, which suggests (see Fig. 1) that TTA formed complexes with Y_2O_3:Eu^{3+} nanoparticles in the form of enolate anion [19]. The band centered at 1638 cm^{-1} is assigned to the H–O–H bending vibration of adsorbed water [20]. However, the ketone group also has an absorption peak at about 1638 cm^{-1}. With the increasing of TTA content, the peak assigned to the ketone group was weakened and the stretching vibrations of chelating carbonyl group (1618 cm^{-1}) [19] increased at the same time. It can be seen in Fig. 4 that the ketone group and chelating carbonyl group had an overlapped wide absorption band. The change in their intensity is a result of the blue shift of the ketone group. Such a blue shift indicated that the ketone group of TTA had reacted with the Eu^{3+} ions on the surface of Y_2O_3:Eu^{3+} nanoparticles and formed a chelating carbonyl group.

Table 1
The calculated crystallite sizes of Y_2O_3:Eu^{3+} nanoparticles.

Sample	Annealing time (h)	Size (nm)
1	2	31.2
2	3	32.1
3	4	33.5
4	5	34.5

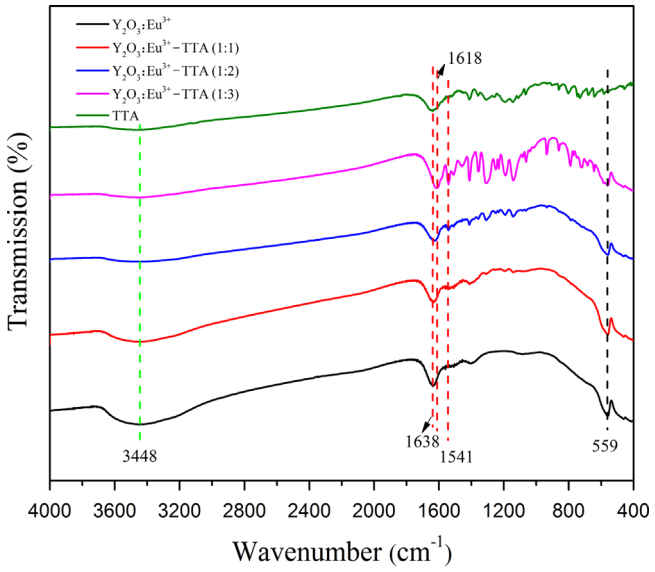

Fig. 4. FTIR spectra of the Y_2O_3:Eu^{3+} nanoparticles capped with different contents of TTA.

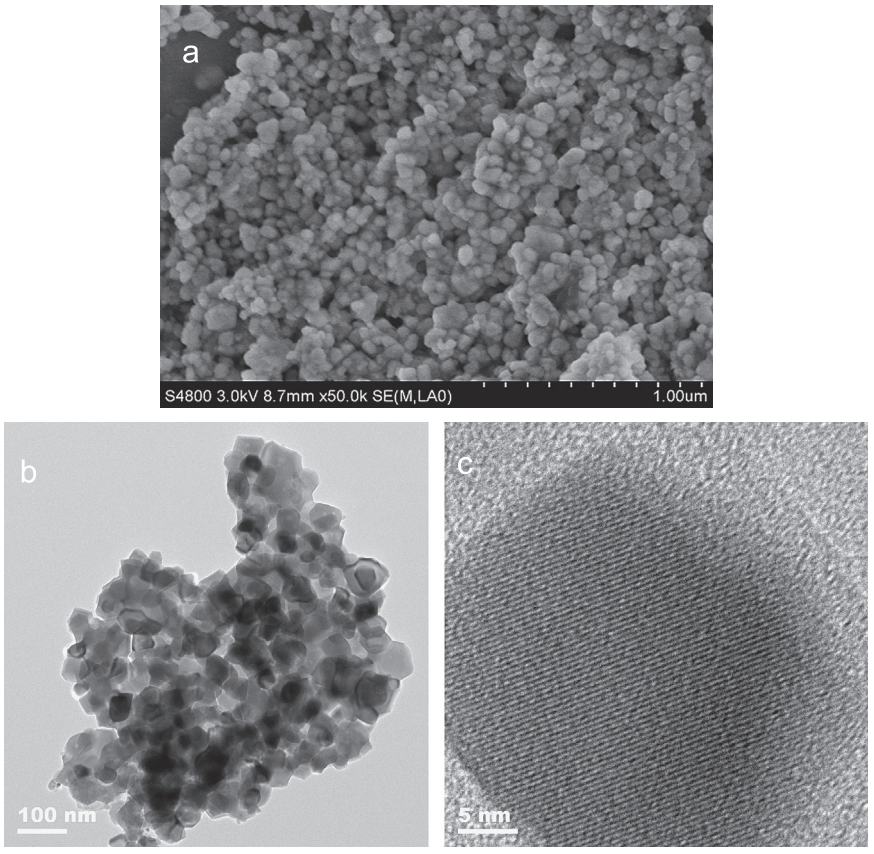

Fig. 3. SEM (a), TEM (b) and HRTEM (c) images of the Y_2O_3:Eu^{3+} nanoparticles.

The band at 3448 cm^{-1} for all the samples can be ascribed to the stretching vibrations of –OH [21]. The –OH functional group, which can lead to luminescence quenching of Eu^{3+} [22], became weaker with the increasing of TTA. This implies that the coordination of TTA with Eu^{3+} ions on the surface of Y_2O_3:Eu^{3+} can eliminate the –OH groups on the surface. Such elimination of –OH groups is beneficial to the improvement of luminescence for the Y_2O_3:Eu^{3+} nanoparticles.

3.3. Luminescence properties

Fig. 5 shows the excitation and emission spectra of the Y_2O_3:Eu^{3+} nanoparticles and Y_2O_3:Eu^{3+}–TTA hybrid nanostructures. As indicated in Fig. 5b, all the emission peaks are characteristic emission of Eu^{3+}, and they are related to the $^5D_0 \rightarrow {}^7F_J$ ($J=1, 2, 3, 4$) transitions of Eu^{3+}.

For the Y_2O_3:Eu^{3+} nanoparticles, the broad excitation band ranging from 200 nm to 285 nm peaking at about 260 nm (Fig. 5a) is attributed to the $O^{2-} \rightarrow Eu^{3+}$ charge transferring (CT), and the characteristic excitation peaks of Eu^{3+} ion can also be clearly seen and are similar to other published results [23,24].

For the Y_2O_3:Eu^{3+}–TTA hybrid nanostructures, a strong broad excitation band which centered at about 368 nm (Fig. 5a) was observed, which is similar to other $Eu(TTA)_3$ complexes as reported by others [25–27]. This broad excitation band is attributed to the strong absorption of TTA in this wavelength range [28]. TTA ligands absorb excitation photons and then transfer their excited electrons to the chelated Eu^{3+} ions for strong emission at 614 nm (Fig. 5b). The strong broad excitation band indicated that TTA effectively sensitized the emission of Eu^{3+} on the surface of Y_2O_3:Eu^{3+} nanoparticles.

It is interesting to note in Fig. 5a that the $O^{2-} \rightarrow Eu^{3+}$ CT band intensity for the Y_2O_3:Eu^{3+}–TTA hybrid nanoparticles was largely weakened by TTA. This can be explained as follows. Both the $O^{2-} \rightarrow Eu^{3+}$ and TTA $\rightarrow Eu^{3+}$ excitation bands are established by the mechanism of charge transfer. They function simultaneously, but they compete against each other. This is reasonable because when TTA transfers an excited electron to a Eu^{3+} ion, it cannot simultaneously accept another excited electron from others due to the repulsive electromagnetic force.

The TTA sensitization process of Y_2O_3:Eu^{3+}–TTA hybrid nanostructures is illustrated in Fig. 6. When the Y_2O_3:Eu^{3+}–TTA hybrid nanostructure is irradiated by UV-light, electrons in the TTA ligand are excited to the first excited singlet state S_1 from the ground state S_0. The excited electrons can relax back to the ground state or the triplet state T_1 via intersystem crossing [19]. Energy can be transferred from the triplet state

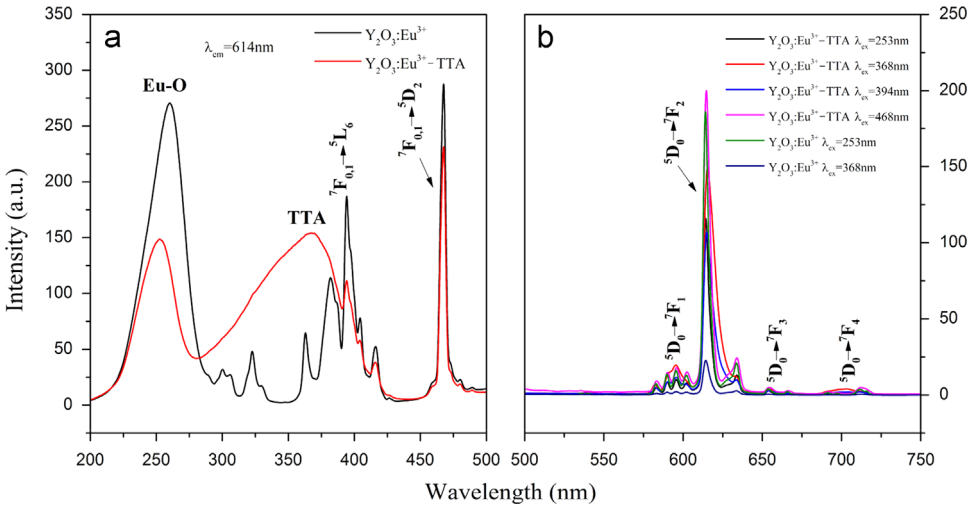

Fig. 5. Excitation (a) and emission (b) spectra of the Y_2O_3:Eu^{3+} and Y_2O_3:Eu^{3+}–TTA hybrid nanoparticles.

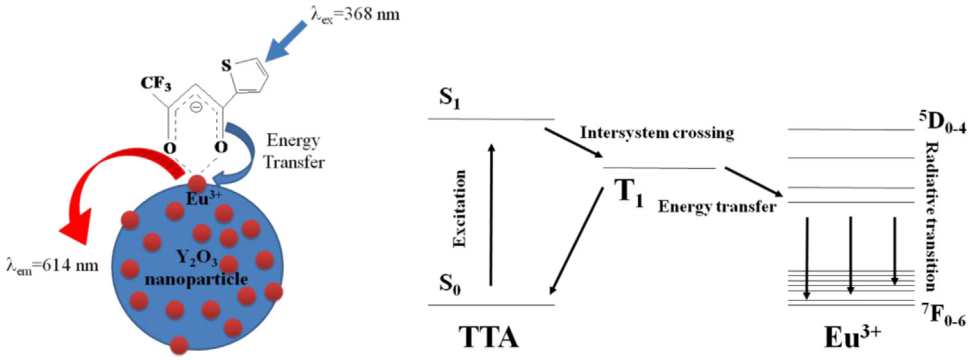

Fig. 6. The sensitization process of Y_2O_3:Eu^{3+}–TTA hybrid nanoparticles.

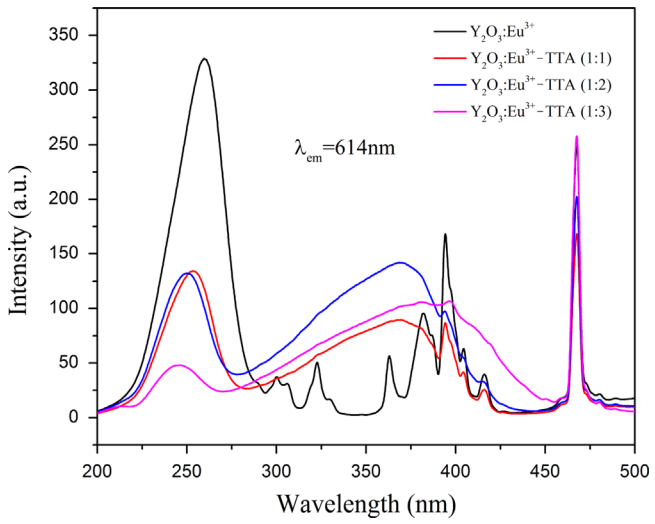

Fig. 7. Excitation spectra of the $Y_2O_3:Eu^{3+}$ capped with different contents of TTA.

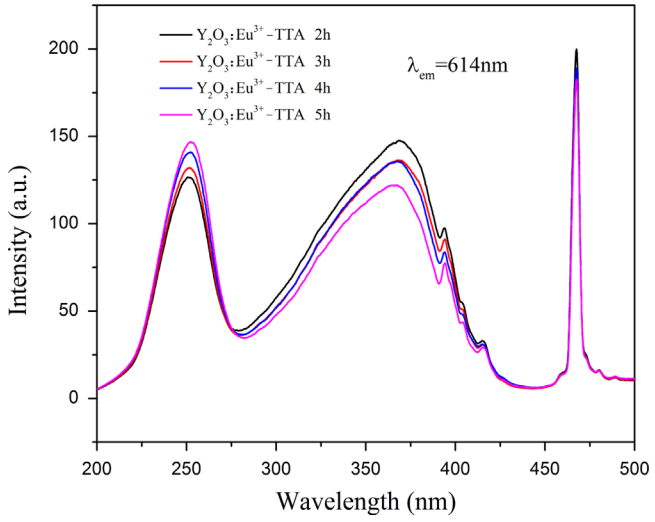

Fig. 8. Excitation spectra of the $Y_2O_3:Eu^{3+}$–TTA hybrid nanostructures (molar ratio 1:1) with different annealing time.

T_1 to the Eu^{3+} via the coordinate bond between TTA and Eu^{3+} [29], and the excited Eu^{3+} ion initiates a radiative transition between ^5D_J level and ^7F_J level.

Fig. 7 shows the excitation spectra of the $Y_2O_3:Eu^{3+}$ capped with different contents of TTA. Similar to the result shown in Fig. 5, the luminescence intensity of $O^{2-}\rightarrow Eu^{3+}$ CT band weakened and the position of $O^{2-}\rightarrow Eu^{3+}$ CT band blue shifted with the increase of TTA content. The luminescence intensity of TTA$\rightarrow Eu^{3+}$ ligand excitation band increased at first and then decreased with the TTA content. In addition, the TTA$\rightarrow Eu^{3+}$ ligand excitation band broadened and red shifted when the molar ratio of $Y_2O_3:Eu^{3+}$ to TTA reached 1:3.

Fig. 8 shows the effect of annealing time on the excitation characteristics of the $Y_2O_3:Eu^{3+}$–TTA hybrid nanostructures (molar ratio at 1:1). The intensity of $O^{2-}\rightarrow Eu^{3+}$ CT band increased with the annealing time. It should be attributed to the reduction of crystalline defects by the annealing for longer time [30]. In contrast, the TTA$\rightarrow Eu^{3+}$ ligand excitation band became weaker with the increase of annealing time. Annealing can generally reduce the specific surface area of nanoparticles by smoothening their surfaces, and therefore less Eu^{3+} ions will be available for the formation of TTA–Eu^{3+} complexes.

4. Conclusions

Cubic $Y_2O_3:Eu^{3+}$ nanoparticles with a size about 32 nm were successfully synthesized using a facile hydrothermal method followed by an annealing process. The $Y_2O_3:Eu^{3+}$ nanoparticles had a broad Eu–O excitation band ranging from 200 nm to 285 nm peaking at about 260 nm. The $Y_2O_3:Eu^{3+}$ nanoparticles were used to prepare the $Y_2O_3:Eu^{3+}$–TTA hybrid nanostructures with TTA. Their chemical bonding information was analyzed by FTIR. The $Y_2O_3:Eu^{3+}$–TTA hybrid nanostructures exhibited a new strong excitation band ranging from 280 nm to 390 nm peaking at about 368 nm. This new excitation band was attributed to the energy transfer mechanism of the $Y_2O_3:Eu^{3+}$–TTA hybrid system. It was found that the Eu–O excitation band became weakened with the increase of TTA contents for the $Y_2O_3:Eu^{3+}$–TTA hybrid nanostructures. These two excitation mechanisms worked against each other. The phase structures, chemical bonding information, microstructural characteristics and luminescence properties were investigated.

Acknowledgments

This work was supported by the Natural Science Foundation of China (Grants 51362020 and 61366004).

References

[1] J. Kido, W. Ikeda, M. Kimura, K. Nagai, White-light-emitting organic electroluminescent device using lanthanide complexes, Japanese Journal of Applied Physics 35 (1996) 394–396.
[2] L.N. Sun, H.J. Zhang, Q.G. Meng, F.Y. Liu, L.S. Fu, C.Y. Peng, J.B. Yu, G.L. Zheng, S.B. Wang, Near-infrared luminescent hybrid materials doped with lanthanide (Ln) complexes (Ln=Nd, Yb) and their possible laser application, The Journal of Physical Chemistry B 109 (13) (2005) 6174–6182.
[3] F. Wang, W.B. Tan, Y. Zhang, X.P. Fan, M.Q. Wang, Luminescent nanomaterials for biological labelling, Nanotechnology 17 (1) (2006) 1–13.
[4] T.L. Phan, M.H. Phan, N. Vu, T.K. Anh, S.C. Yu, Luminescent properties of Eu-doped Y_2O_3 nanophosphors, Physica Status Solidi A 201 (9) (2004) 2170–2174.
[5] P.A. Tanner, K.L. Wong, Synthesis and spectroscopy of lanthanide ion-doped Y_2O_3, The Journal of Physical Chemistry B 108 (1) (2004) 136–142.
[6] W.F. Chen, Y.P. Tong, Y. Liu, M. Liu, Y.C. Lin, B. Gong, Z.S. Cai, X. L. Zhong, Facile synthesis and luminescent properties of Y_2O_3: Eu^{3+} nanophosphors via thermal decomposition of cocrystallized yttrium europium propionates, Ceramics International 39 (4) (2012) 3741–3745.
[7] L.R. Singh, R.S. Ningthoujam, V. Sudarsan, I. Srivastava, S.D. Singh, G. K. Dey, S.K. Kulshreshtha, Luminescence study on Eu^{3+} doped Y_2O_3 nanoparticles: particle size, concentration and core-shell formation effects, Nanotechnology 19 (5) (2008) 055201.
[8] Y.C. Kang, H.S. Roh, D.J. Seo, S.B. Park, The effect of metal carbonate fluxes on the crystallinity, morphology, and photoluminescence

characteristics of Y_2O_3:Eu phosphor in spray pyrolysis, Journal of Materials Science Letters 19 (14) (2000) 1225–1227.
[9] F.W. Liu, C.H. Hsu, F.S. Chen, C.H. Lu, Microwave-assisted solvothermal preparation and photoluminescence properties of Y_2O_3:Eu^{3+} phosphors, Ceramics International 38 (2) (2012) 1577–1584.
[10] G. Wakefield, E. Holland, P.J. Dobson, J.L. Hutchison, Luminescence properties of nanocrystalline Y_2O_3:Eu, Advanced Materials 13 (20) (2011) 1557–1560.
[11] S.W. Li, Z.Y. Hou, Z.Y. Cheng, H.Z. Lian, P.A. Ma, C.X. Li, J. Lin, Enhanced near-infrared quantum cutting luminescence in 1, 2, 4, 5-benzenetetracarboxylic acid/$NaYF_4$: Tb^{3+}, Yb^{3+} hybrid nanoparticles, RSC Advances 3 (16) (2013) 5491–5497.
[12] X.C. Wen, Y.L. Zhao, L.M. Wang, M. Zhang, D.Q. Gao, Synthesis and fluorescence properties of europium, terbium doped Zn^{2+}, Cd^{2+} and Cr^{3+} complexes, Journal of Rare Earths 25 (6) (2007) 679–683.
[13] B. Kokuoz, C. Kucera, J.R. DiMaio, J. Ballato, Organic–inorganic hybrid nanoparticles with enhanced rare-earth emissions, Optical Materials 31 (9) (2009) 1327–1330.
[14] Z. Rzączyńska, A. Ostasz, M. Sikorska-Iwan, H. Głuchowska, E. Olszewska, S. Pikus, Synthesis and characterization of metal polycarboxylates constructed from lanthanides (iii) and 1, 2, 4, 5-benzenetetracarboxylic acid, Journal of Thermal Analysis and Calorimetry 84 (3) (2006) 575–579.
[15] M.H.V. Werts, M.A. Duin, J.W. Hofstraat, J.W. Verhoeven, Bathochromicity of Michler's ketone upon coordination with lanthanide (III) β-diketonates enables efficient sensitisation of Eu^{3+} for luminescence under visible light excitation, Chemical Communications 9 (1999) 799–800.
[16] K. Binnemans, Rare-earth beta-diketonates, Handbook on the Physics and Chemistry of Rare Earths 35 (2005) 107–272.
[17] J. Goldstein, D.E. Newbury, D.C. Joy, C.E. Lyman, P. Echlin, E. Lifshin, L. Sawyer, J.R. Michael, Scanning Electron Microscopy and X-ray Microanalysis, Springer, Berlin, 2003.
[18] Y.P. Fu, Preparation and characterization of Y_2O_3:Eu phosphors by combustion process, Journal of Materials Science 42 (13) (2007) 5165–5169.
[19] J.C. Chen, Q.G. Meng, P.S. May, M.T. Berry, C.K. Lin, Sensitization of Eu^{3+} luminescence in Eu:YPO_4 nanocrystals, The Journal of Physical Chemistry C 117 (11) (2013) 5953–5962.
[20] M. Falk, The frequency of the H–O–H bending fundamental in solids and liquids, Spectrochimica Acta 40A (1) (1984) 43–48.
[21] S. Knop, T.L.C. Jansen, J. Lindner, P. Vöhringer, On the nature of OH-stretching vibrations in hydrogen-bonded chains: Pump frequency dependent vibrational lifetime, Physical Chemistry Chemical Physics 13 (10) (2011) 4641–4650.
[22] Y.C. Yan, A.J. Faber, H. De Waal, Luminescence quenching by OH groups in highly Er-doped phosphate glasses, Journal of Non-Crystalline Solids 181 (3) (1995) 283–290.
[23] Y.C. Kang, S.B. Park, I.W. Lenggoro, K. Okuyama, Preparation of nonaggregated Y_2O_3:Eu phosphor particles by spray pyrolysis method, Journal of Materials Research 14 (6) (1995) 2611–2615.
[24] J. Yang, Z.W. Quan, D.Y. Kong, X.M. Liu, J. Lin, Y_2O_3:Eu^{3+} microspheres: solvothermal synthesis and luminescence properties, Crystal Growth and Design 7 (4) (2007) 730–735.
[25] J. Kai, D.F. Parra, H.F. Brito, Polymer matrix sensitizing effect on photoluminescence properties of Eu^{3+}-β-diketonate complex doped into poly-β-hydroxybutyrate (PHB) in film form, Journal of Materials Chemistry 18 (38) (2008) 4549–4554.
[26] H.R. Li, H.J. Zhang, J. Lin, S.B. Wang, K.Y. Yang, Preparation and luminescence properties of ormosil material doped with Eu $(TTA)_3$ phen complex, Journal of Non-Crystalline Solids 278 (1) (2000) 218–222.
[27] C.K. Lin, M.T. Berry, P.S. May, Influence of colloidal-gold films on the luminescence of Eu $(TTFA)_3$ in PMMA, Journal of Luminescence 130 (10) (2010) 1907–1915.
[28] P.A. Tanner, B. Yan, H.J. Zhang, Preparation and luminescence properties of sol–gel hybrid materials incorporated with europium complexes, Journal of Materials Science 35 (17) (2000) 4325–4328.
[29] J.B. Guan, B. Chen, Y.Y. Sun, H. Liang, Q.J. Zhang, Effects of synergetic ligands on the thermal and radiative properties of Eu $(TTA)_3$nL-doped poly (methyl methacrylate), Journal of Non-Crystalline Solids 351 (10) (2005) 849–855.
[30] J.W. Lee, H. Shichijo, H.L. Tsai, R.J. Matyi, Defect reduction by thermal annealing of GaAs layers grown by molecular beam epitaxy on Si substrates, Applied Physics Letters 50 (1) (1987) 31–33.